

Chapter 6

Lens-less Off-axis Self-Referencing Digital Holographic Microscopy

6.1 Introduction

With the rapid growth of computing and display technologies digital holography has undergone significant advancement in the past several decades [66,67,184,206,207,273]. It has been already known that digital holography is deployed in scientific, engineering and biomedical application [22,28,60,288–290]. Apart from that, digital holography is also incorporated in number of contemporary applications such as holographic cryptography, optical metrology, remote sensing and inspection etc [291,292]. Traditionally a digital holographic microscope makes use of lenses and opto-mechanical parts, together with alignment mechanics. Because of these factors, the imaging system is hard to be operated in an on-field setting. Moreover, there is an inherent trade-off between resolution and FOV in any imaging system where the two are coupled. It means that to observe finer details with better resolution, results in relatively smaller FOV [139].

Also, lenses are used in these setups for imaging the samples under study. However, holography invented by Gabor in 1948 was a lens-free imaging technique in which in-line holograms were observed [182,293–295]. Twin image problem occurred in the in-line hologram that was resolved by Leith and Upatnieks by developing Off-axis holography [67,266,269,294–297]. To attain high-resolution imaging lenses are used, however lens-less imaging is serviceable where high resolution is not a major requirement [77,137–139,298–306]. Chromatic and optical aberrations due to lenses distort the image that is a tedious to remove computationally [142,307–314]. Also, smaller FOV is obtained (compared to lens-less case) for the systems equipped with magnifying lenses. To remove these discrepancies a lens-less off-axis microscope is required that is suitable for large FOV studies along with single shot operation. Further, the lens-less microscope would be compact, easy to implement, portable, and robust that can even be used in remote locations.

This chapter provide details of the development of an off-axis, lens-less, self-referencing digital holographic microscope that is easy to operate and compact. The lens-less setups have already been used for different imaging applications such as in searching of microbes [293,315], for bio-pharmaceutical application [316], in air quality monitoring [317], and sperm cell analysis

etc. [58,137,293,304]. In the chapter, development an off-axis lens less microscope employing Laser diodes and LED sources are described. The developed microscope works on the principle of Digital Holography involving Lateral Shearing Interferometer and Fresnel biprism. USAF high-resolution target and phase objects are imaged using the microscope to test its effectiveness.

6.2 Lens-less Common path Off-axis Digital Holographic Microscope

The setup is shown in Fig. 6.1 and 6.2 is based on lateral shearing geometry which is uses amplitude division interferometry. The lens which is generally used in conventional microscopy systems, is omitted in the setup (Fig 6.2) making the whole imaging process free from aberrations caused by lenses. Lens less digital holographic microscopy system shown in Fig. 6.2 provides single-shot, large FOV quantitative phase imaging of phase objects. . Employing a lens less digital holographic microscope configuration allows the system to be compact and robust, but typically comes with performance tradeoffs, e.g. sample very close to the detector array [113,318–322] can provide a larger FOV with high lateral resolution. However, in such a case introduction of a separate off-axis reference beam, which allows single shot quantitative phase reconstruction, is almost impossible. The setup shown in Fig.6.1 and 6.2 allows introduction of an off-axis reference beam, enabling single-shot quantitative phase imaging at the cost of resolution, and smaller FOV compared to Gabor lens-less digital holographic microscopy [139,140]. The setup investigate is robust, compact, field deployable, cost-effective, and has single-shot imaging capability. It does not require mechanical focusing for obtaining depth information, all the data can be retrieved from a single hologram.

The investigated lens-less off-axis common path DHM using lateral shearing interferometer employs laser diodes as the source of illumination. A portion of the laser beam illuminate sample and the region not perturbed by sample information acts as the reference. A shearing plate splits the wave into two, the wave propagating from the front and the back of the plate then interferes at the CCD plane to form a hologram. The setup is temporally stable as both reference and object wave pass through the same environment that makes it suitable for dynamic studies.

6.3 Theoretical background

During recording of holograms, a spherical wavefront (Fig. 6.1b) is used for illumination of the sample. However, the numerical reconstruction assumes a plane reference wavefront [305]. This leads to the distance of the virtual/real image of the object from the hologram plane,

shifting from the location where the object was located as resulting in geometrical magnification [182,305]. Hence, numerical reconstruction at best focus plane requires, determination of the image locations and transverse magnification considering plane reference wavefront.

Fig. 6.1b shows the co-ordinate system used to determine the reconstruction distance as well as transverse magnification of the lateral shearing lens less digital holographic microscope. Assume the reference wave is generated by a single point source S_r at (x_r, y_r, z_r) at a distance z_r from the digital array. Owing to the lateral shearing geometry, it can be seen from Fig. 6.1b that the sample is illuminated by a point source S_o , located at a distance L from the detector array. Theoretically, it suffices to consider only a single point source at (x_o, y_o, z_o) at a distance of $(L-z)$ from the detector plane.

During the reconstruction, the hologram is assumed to be illuminated by a spherical beam originating from a point source $S_p(x_p, y_p, z_p)$ located at a distance z_p from the detector array. The paraxial approximations to the twin image locations for an object point source at the given coordinates will be determined by the analysis. A collection of such mutually coherent point sources can then be considered an extended coherent object.

Considering the case in which the locations of the reference point source and object point source are located at distance z_r from the hologram plane, the total field incident on the recording plane is represented by (where x and y are the lateral coordinates of the sensor plane):

$$U(x, y) = A \exp\left\{-j \frac{\pi}{\lambda_1 z_r} [(x - x_r)^2 + (y - y_r)^2]\right\} + a \exp\left\{-j \frac{\pi}{\lambda_1 z_o} [(x - x_o)^2 + (y - y_o)^2]\right\} \quad (6.1)$$

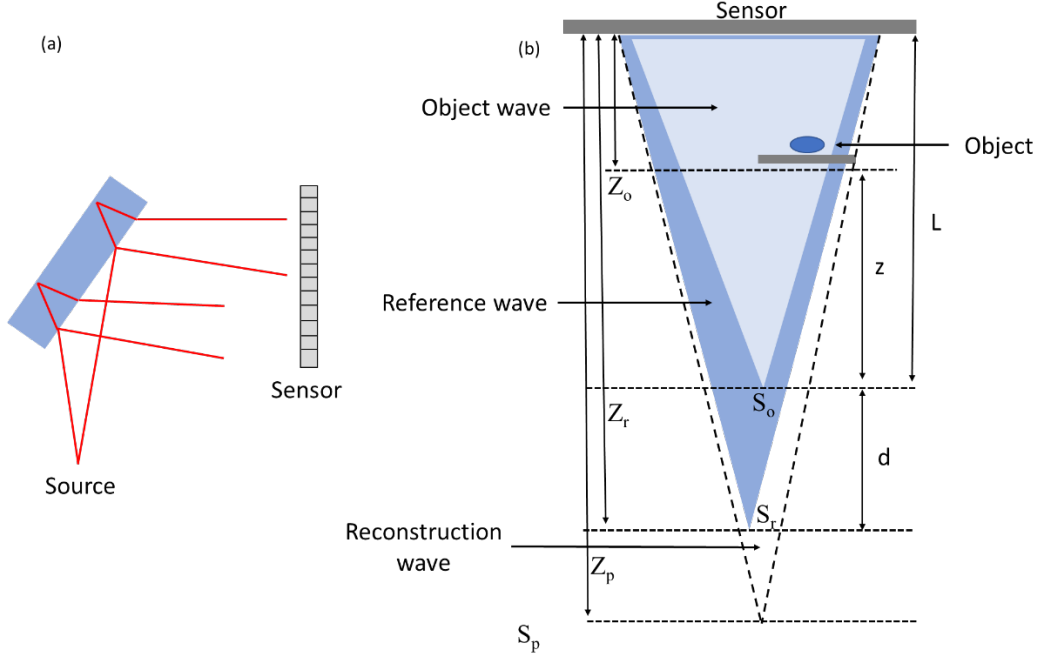


Fig 6.1 (a) The hologram recording from the beams after passing through shearing (b) Unfolding of the interference pattern formation in the off-axis Lens-less digital holographic microscope

Complex constants are represented by A and a , representing the amplitudes and relative phases of the two spherical waves. The below equation represents the corresponding intensity due to two waves

$$I(x, y) = |A|^2 + |a|^2 \quad (6.2)$$

Below two equations represent the two transmittance terms that represent the twin images assuming that the amplitude transmittance of the resulting hologram is proportional to the exposure,

$$t_3 = \beta' Aa * \exp \left\{ -j \frac{\pi}{\lambda_1 Z_r} [(x - x_r)^2 + (y - y_r)^2] + j \frac{\pi}{\lambda_1 Z_o} [(x - x_o)^2 + (y - y_o)^2] \right\}$$

$$t_4 = \beta' Aa * \exp \left\{ j \frac{\pi}{\lambda_1 Z_r} [(x - x_r)^2 + (y - y_r)^2] - j \frac{\pi}{\lambda_1 Z_o} [(x - x_o)^2 + (y - y_o)^2] \right\} \quad (6.3)$$

If the hologram is illuminated by a spherical wave during reconstruction, which in the paraxial approximation is described by

$$U_p = (x, y) = B \exp \left\{ -j \frac{\pi}{\lambda_2 Z_p} [(x - x_p)^2 + (y - y_p)^2] \right\} \quad (6.4)$$

The two wavefronts of interest behind the hologram are found by multiplying Eq. (6.3) and Eq. (6.4) yielding.

$$U_3(x, y) = t_3 B \exp \left\{ -j \frac{\pi}{\lambda_2 Z_p} [(x - x_p)^2 + (y - y_p)^2] \right\}$$

$$U_4(x, y) = t_4 B \exp \left\{ -j \frac{\pi}{\lambda_2 Z_p} [(x - x_p)^2 + (y - y_p)^2] \right\} \quad (6.5)$$

According to Eq. (6.5), the wavefront scattered from hologram structures is given by a product of quadratic exponentials. This means that the scattered reference wavefront should also be represented using quadratic exponentials. Thus, the coordinates (x_i, y_i, z_i) of the images can be determined by comparing the expanded equation Eq. (6.5) with a quadratic exponential like one given below:

$$U_i(x, y) = K \exp \left\{ -j \frac{\pi}{\lambda_1 Z_i} [(x - x_i)^2 + (y - y_i)^2] \right\} \quad (6.6)$$

Comparing the coefficients of the quadratic terms the axial distance z_i of the image point from the hologram plane can be written as

$$Z_i = \left(\frac{1}{Z_p} \pm \frac{1}{Z_r} \mp \frac{1}{Z_o} \right)^{-1} \quad (6.7)$$

Where the upper set of signs applies for one image and the lower set of signs for the other. When Z_i is negative, the image is virtual and lies to the left of the hologram plane, while when Z_i is positive, the image is real and lies to the right of the hologram plane. If the reconstruction wave is considered as a plane wave, then $Z_p = \infty$ which gives the axial distance of the image location from the hologram plane as

$$Z_i = \left(\frac{1}{Z_r} - \frac{1}{Z_o} \right)^{-1} \quad (6.8)$$

Considering Fig. 6.2b for lateral shearing off-axis lens less geometry, in which the spherical waves leading to the formation of holograms are located at different axial points, Eq. (6.8) has to be modified considering $Z_r = (L+d)$ and $Z_o = (L-z)$. This leads to the image point location for the developed microscope as

$$Z_i = \left(\frac{1}{L+d} - \frac{1}{L-z} \right)^{-1}$$

$$Z_i = \frac{(L+d)(L-z)}{(z+d)} \quad (6.9)$$

Where L denotes distance between the sensor and the object point source, z denotes the distance between the source and the object and d denotes the distance between the reference point and the object source point.

6.3.1 Axial and Transverse Magnifications

The image coordinates can further be used for the calculation of axial and transverse magnifications which are given by

$$M_T = \left| \frac{z_i}{z_o} \right| = \left| 1 - \frac{z_o}{z_r} \right|^{-1} = \left| 1 - \frac{L-z}{L+d} \right|^{-1} = \left| \frac{L+d}{z+d} \right| \quad (6.10)$$

$$M_A = (M_T)^2 \quad (6.11)$$

The x and y coordinates of the image points are found by equating the linear terms in x and y in Eq. (6.5) and Eq. (6.6), with the result

$$x_i = \mp \frac{Z_i}{Z_o} x_o \pm \frac{Z_i}{Z_o} x_r + \frac{Z_i}{Z_p} x_p$$

$$y_i = \mp \frac{Z_i}{Z_o} y_o \pm \frac{Z_i}{Z_o} y_r + \frac{Z_i}{Z_p} y_p \quad (6.12)$$

Eq. (6.10), (6.11) and (6.12) provide the fundamental relations that allows prediction of the location of the images of point sources created by the holographic process.

6.4 Experimental Setup

The diagram of the developed lens-less microscope is shown in Fig 6.2. The system is made as compact as possible. A Laser diode module (Thorlabs, $\lambda=635\text{nm}$, max output power 1.2mW) is used as the illumination source. A diverging beam is produced by using a MO lens (Melles Griot, 45x, NA 0.65). A mirror is placed at an angle of 45° with respect to the beam which directs it towards the object under investigation. The beam interacts with the object and passes through the shearing plate (5mm thickness) that splits the beam into two. The beam from the front and the back surface of the shearing glassplate then interferes on the CMOS sensor (Thorlabs, pixel pitch $2.2\mu\text{m}$) giving rise to creation holograms. The total distance between the source and the detector is 7cm. The sample to be imaged is positioned at a distance of 3cm from the detector array. Fig 6.3a shows the 3D schematic of the developed microscope and 6.3b shows the actual microscope in the laboratory employing laser diode module along with a CMOS sensor.

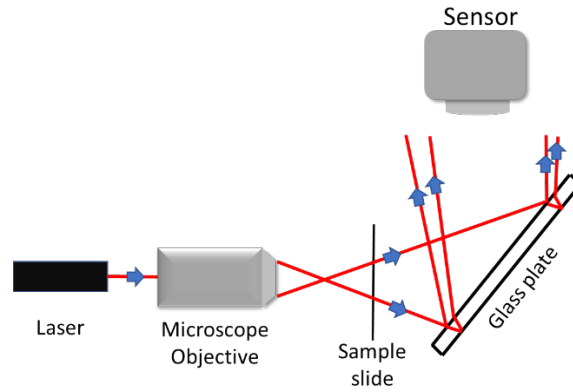


Fig 6.2 Schematic of the Lens-less off axis common path DHIM based on lateral shearing interferometer employing laser diode

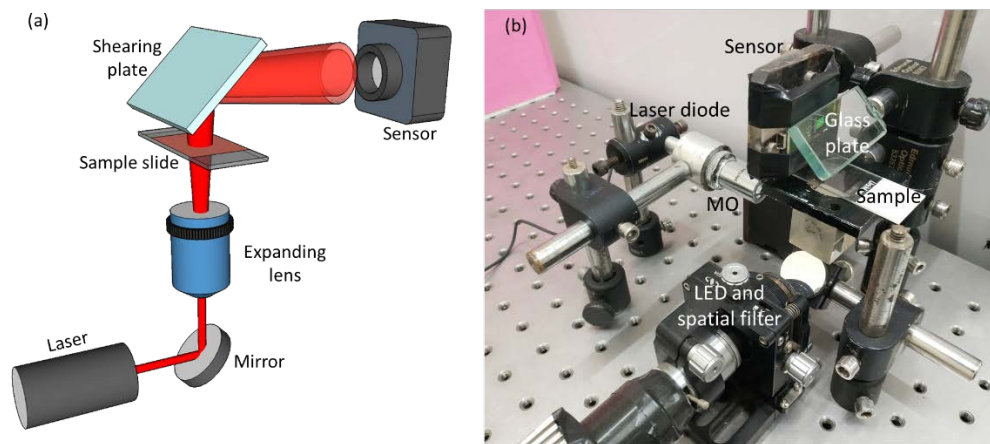


Fig 6.3 (a) 3D schematic of the developed lens less microscope employing lateral shearing interferometer and a laser diode module (b) Photograph of the lens-less microscope in the lab.

6.5 Result and Discussion

6.5.1 Temporal stability

The temporal stability of the system is determined by recording a time series of holograms (25Hz, 30s). Each hologram is numerically reconstructed considering plane reference wavefront and the phase distribution at each time instance is extracted. Spatial mean of standard deviation of the time variation of phase acts as the spatial stability quantifier. The presented setup provides temporal stability of 0.6 nm (Fig. 6.4) without the need of vibration isolation demonstrating that it is more immune to external mechanical noise compared to two-beam setups.

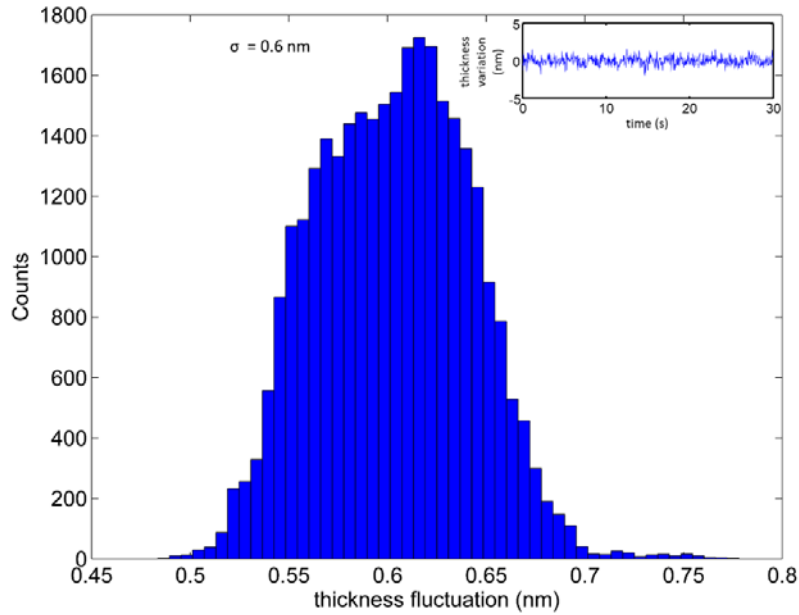


Fig 6.4 Temporal stability of the system. Histogram represents the measured counts for thickness fluctuation at spatial points (standard deviation of time varying thickness). The mean of these values represents the temporal stability of the device. Inset shows the time varying thickness at a spatial point in the field of view.

6.5.2 System Calibration and imaging capability:

The microscope is calibrated using a high-resolution USAF target of known parameters. The recorded hologram of the USAF target is shown in Fig 6.5a. Area of interest in the rectangular region is shown in Fig. 6.5b. The location of the best focus plane is determined using auto-focusing algorithms [323]. Fig 6.6 a to c shows the numerical focusing of the scattered reference wavefront using Angular Spectrum Propagation diffraction integral. The object phase is extracted from a single hologram (Fig. 6.6c), after digitally subtracting the spherical component (Fig. 6.6e) present at the reconstruction plane and is represented in Fig. 6.6f.

In the next set of experiments, dots made by a marker (amplitude objects) on the microscope slide are used as the test specimen and holograms of this sample is recorded using the microscope. Fig 6.7a shows the recorded hologram. Numerical propagation to the best focus plane yields the intensity distribution at this plane as represented in Fig. 6.7c.

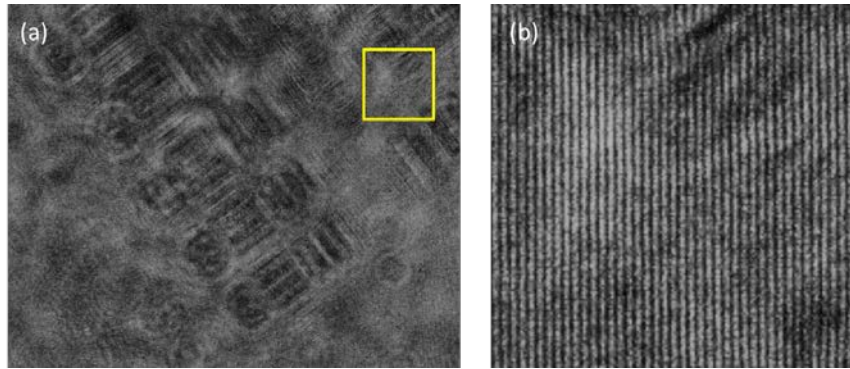


Fig 6. 5 (a) Hologram of the USAF target (b) interference fringes in the marked yellow box in 6.5a

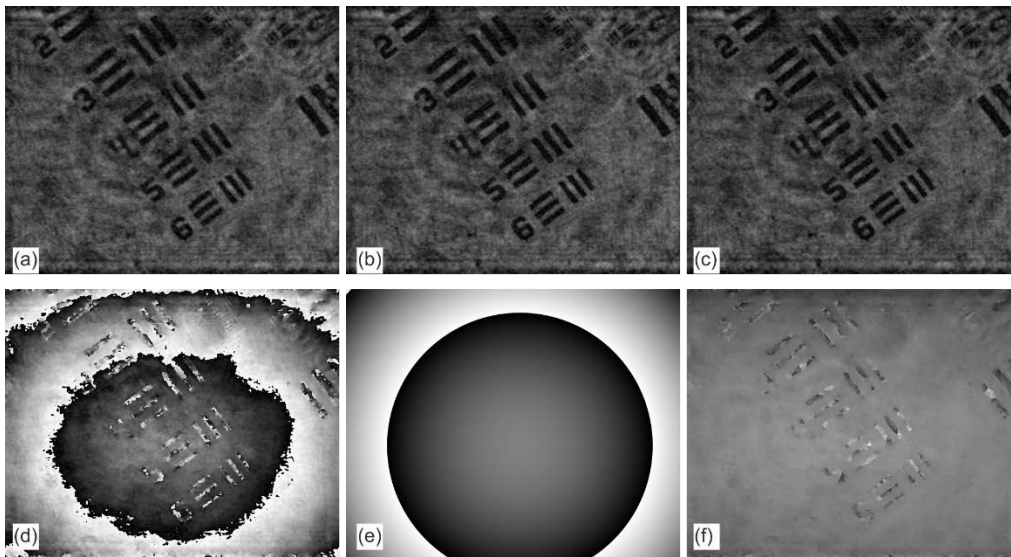


Fig 6.6 (a) to (c) Numerical focusing (a) inside best focus, (b) at best focus (c) outside best focus. (d) Numerically reconstructed wrapped phase distribution at the best focus plane. (e) Digitally subtracted spherical phase factor. (f) Object phase obtained after digital phase compensation.

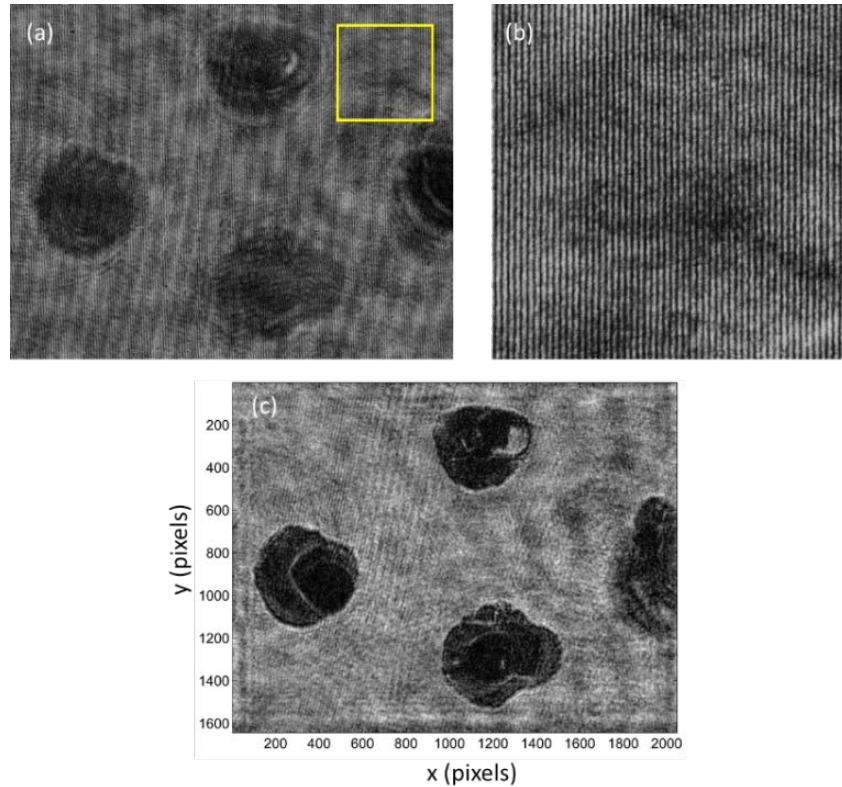


Fig 6.7 (a) Hologram of ink dots on microscope slide (b) Interference fringes inside the region of interest (c) reconstructed intensity at the best focus plane

6.5.3 Quantitative phase imaging of phase micro-objects

To determine the capability of the lateral shearing lens less digital holographic microscope in quantitative phase imaging of phase objects, holograms of structures (a dash and a dot) made on a microscope slide by a permanent red marker pen ink are recorded by illuminating it with a laser source ($\lambda=745$ nm). The distance of the point laser source (fibre output) to the sample is 40mm. Holograms are recorded using a CCD array with $4.65\mu\text{m}$ pixel pitch and is shown in Fig 6.8a. Distance from the sample to the CCD array is 90mm. Autofocusing algorithm based on determination of variance of gray value is used to determine the best focus plane [323]. The best focus plane lies 237.8mm from the hologram plane (Fig. 6.9). Reconstructed intensity and phase at the best focus plane is shown in Fig. 6.9b and 6.9c respectively. The spherical phase is deducted from the object phase shown in Fig 6.8 (d). The object phase after unwrapping and tilt phase subtraction is shown in Fig 6.8 (e). The 3D object phase distribution is obtained shown in Fig 6.8 (f).

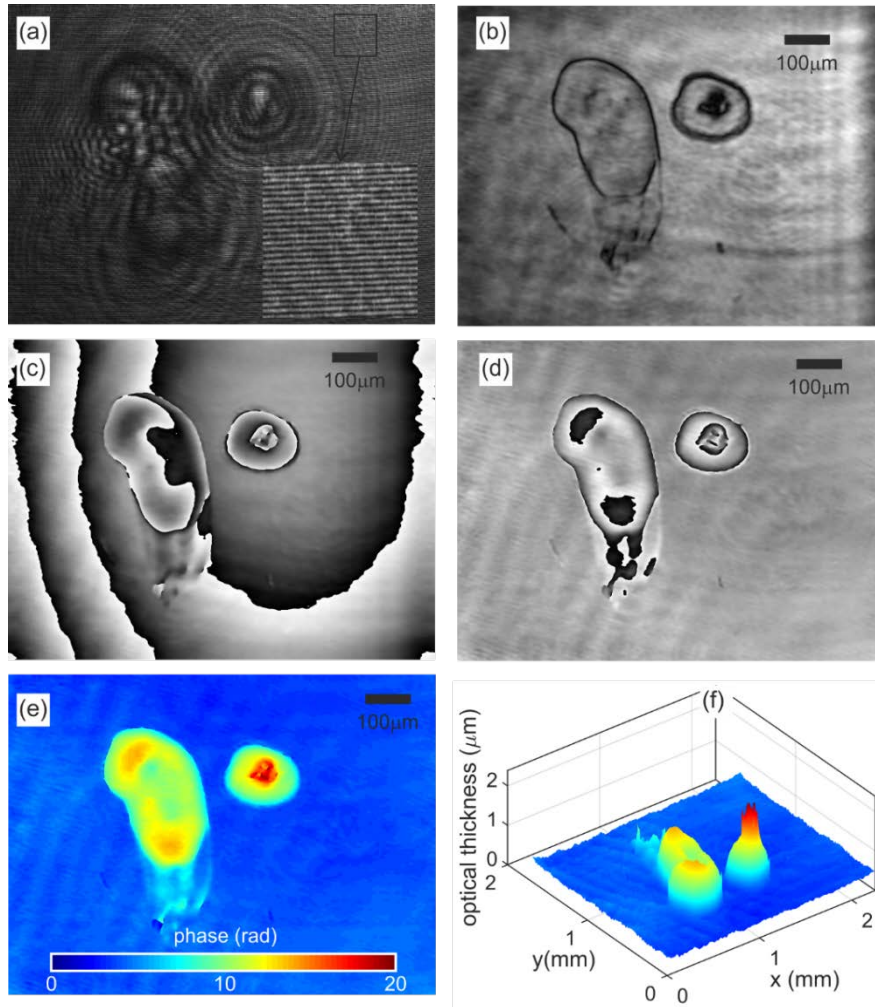


Fig 6.8 (a) Hologram of numbers written on a microscope slide using a marker pen (b) Reconstructed Intensity profile (c) Reconstructed Phase distribution profile (d) Object phase after subtraction of spherical phase (e) Object phase after unwrapping and tilt phase subtraction (f) Three-dimensional rendering of object phase distribution

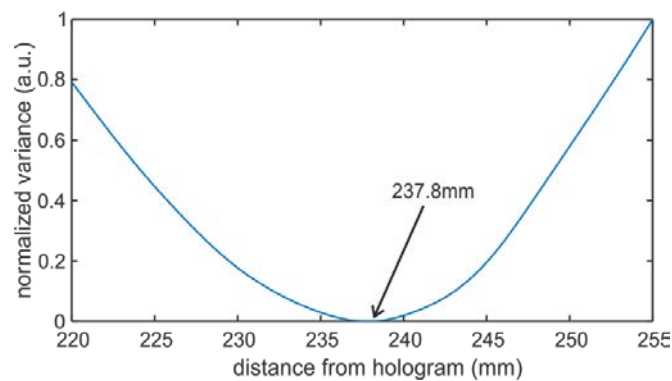


Fig 6.9 Determination of best focus plane using autofocus algorithm based on the variance of reconstructed intensity distribution

6.6 Off-axis lens less digital holographic microscopy using LED and Fresnel biprism

Incorporating LED in lateral shearing geometry with thick glass plates, as discussed in the previous chapter is difficult owing to low temporal coherence of the source. However, Fresnel

biprism, which is ideal for automatic path length matching of object and reference wavefronts could be used along with LED sources in lens less digital holographic microscopy. Fig. 6.10 shows the schematic of the lens less microscope devised using LED sources. It comprises of a light emitting diode (LED) ($\lambda=627$ nm, Luxeon star, max output power=2W, emitting area 1 mm²) as the illuminating light source. The low spatial coherence of the LED is improved with the help of a spatial filter assembly, which reduces its size thereby increasing its spatial coherence area. To increase the effective FOV, a pair of Fresnel biprism (176°, 4cm x 5cm) with the same specifications are placed parallel to each other to generate two sets of interference patterns (multiplexed holograms) which are recorded simultaneously by the CCD array (8-bit, 4.65µm pixel pitch). Here unlike in the case of lateral shearing geometry, the point sources illuminating the sample and acting as the reference wavefront lies at the same distance from the detector plane ($d=0$ in Fig. 6.1b). So, the distance of the image plane from the hologram plane then can be computed from

$$Z_i = \frac{L}{z}(L - z) \quad (6.13)$$

Lateral magnification of the system can be expressed as

$$M_T = \frac{L}{z} \quad (6.14)$$

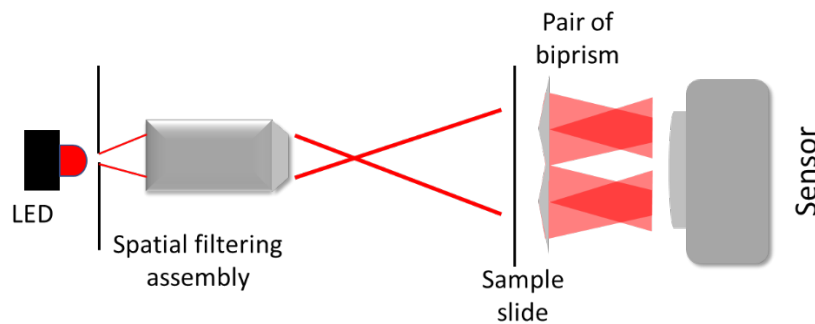


Fig 6.10 shows the 2D schematic of the developed microscope a pair of Fresnel Biprism as an interferometer and a LED ($\lambda=627$ nm, Luxeon star, max output power=2W, emitting area 1 mm²) as the light source

6.6.1 Result and discussion

High-resolution USAF target of known parameters is used to investigate lens-less microscope employing Fresnel Biprism and LED as the light source. Recorded hologram of the USAF target shown in 6.11 a. As in the case using a laser source, the best focus plane is found by using autofocusing algorithms. The reconstructed phase of the USAF resolution target at the best focus plane is shown in Fig. 6.11b. Three-dimensional rendering of the continuous phase distribution of the object at the best focus plane is shown in Fig. 6.11c.

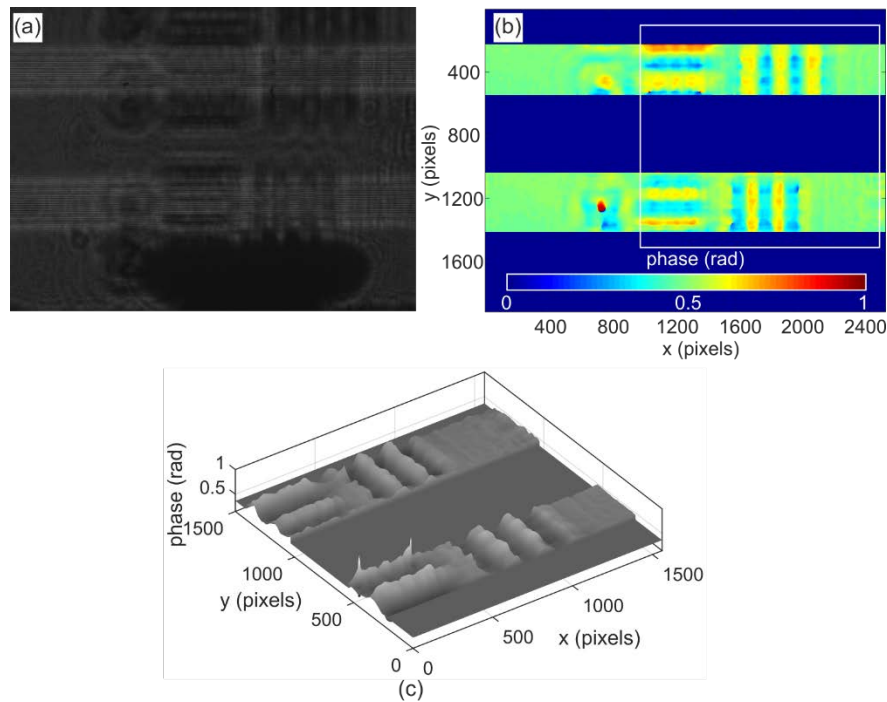


Fig 6.9 (a) hologram of the USAF target recorded using the lens-less microscope using LED source and a pair of Fresnel biprisms (b) reconstructed continuous phase distribution at the best focus plane (c) the 3D rendering of the spatially varying object phase distribution

6.7 Conclusion

This work described in this chapter demonstrates development of off-axis, lens-less, self-referencing microscope that can image amplitude and phase samples. The demonstrated devices are compact, easy to operate and field deployable. As discussed in the chapter, microscopy with lens and without lens can be used for observing specimens and both have their own merits and demerits. To attain high-resolution imaging, lenses (especially with visible light) are necessary, nevertheless lens-less imaging is serviceable where high resolution is not a major requirement. The use of lens and other optical components introduce aberration in the system. Removing the lens can reduce the effect of aberration and provide larger FOV than microscopes employing lenses. The developed system utilizes lesser number of components compared to other microscopes based on interferometry which improves its temporal stability by making it immune to external mechanical vibration and reduces its form factor. The developed microscope works on the principle of Digital Holography involving Lateral Shearing Interferometer and Fresnel biprism. USAF high-resolution target and phase objects are imaged using the microscope to test its effectiveness. The value of temporal stability is found to be 0.6 nm over a period of 30s. The microscope works on the principle of self-referencing Digital Holography. Lens less device based on lateral shearing interferometer, is ideal for use along with laser sources, giving high contrast interference fringes in the entire FOV, making it useful

for large FOV quantitative phase imaging. However, with LED sources, lateral shearing interferometer using a shearing plate (glass plate) is difficult to implement, due to the low coherence length of the source, which is much less than the pathlength difference introduced by the glass plate. Use of LED required a self-refencing technique, which can automatically match the path length of the object and reference beams. This is achieved by using Fresnel biprism. However, the FOV generated by a single biprism is again limited by the coherence length of the LED source. Improved FOV is achieved by using a pair of biprisms, which generates two independent FOV (regions with interference pattern), which are recorded by the same CCD array (hologram multiplexing). Even though biprism generates shearing pattern it will not interfere with the usable field of view since the path length between the sheared beams will be larger than the coherence length of the source (LED). The developed microscope can provide a multitude of sample parameters based on its morphology and along with effective machine learning algorithms, might be useful in on-filed sample classification.